nature COMMUNICATIONS

ARTICLE

Received 4 Apr 2012 | Accepted 1 Aug 2012 | Published 11 Sep 2012

DOI: 10.1038/ncomms2042

Proximity-induced high-temperature superconductivity in the topological insulators Bi_2Se_3 and Bi_2Te_3

Parisa Zareapour[1,*], Alex Hayat[1,2,*], Shu Yang F. Zhao[1], Michael Kreshchuk[1], Achint Jain[1], Daniel C. Kwok[3], Nara Lee[3], Sang-Wook Cheong[3], Zhijun Xu[4], Alina Yang[4], G.D. Gu[4], Shuang Jia[5], Robert J. Cava[5] & Kenneth S. Burch[1]

Interest in the superconducting proximity effect has been reinvigorated recently by novel optoelectronic applications as well as by the possible emergence of the elusive Majorana fermion at the interface between topological insulators and superconductors. Here we produce high-temperature superconductivity in Bi_2Se_3 and Bi_2Te_3 via proximity to $Bi_2Sr_2CaCu_2O_{8+\delta}$, to access higher temperature and energy scales for this phenomenon. This was achieved by a new mechanical bonding technique that we developed, enabling the fabrication of high-quality junctions between materials, unobtainable by conventional approaches. We observe proximity-induced superconductivity in Bi_2Se_3 and Bi_2Te_3 persisting up to at least 80 K—a temperature an order of magnitude higher than any previous observations. Moreover, the induced superconducting gap in our devices reaches values of 10 mV, significantly enhancing the relevant energy scales. Our results open new directions for fundamental studies in condensed matter physics and enable a wide range of applications in spintronics and quantum computing.

[1] Department of Physics and Institute for Optical Sciences, University of Toronto, 60 St George Street, Toronto, Ontario, Canada M5S 1A7. [2]Centre for Quantum Information and Quantum Control, University of Toronto, 60 St George Street, Toronto, Ontario, Canada M5S 1A7. [3]Rutgers Center for Emergent Materials and Department of Physics and Astronomy, Rutgers University, Piscataway, New Jersey 08854, USA. [4] Department of Condensed Matter Physics and Materials Science (CMPMS), Brookhaven National Laboratory, Upton, New York 11973, USA. [5]Department of Chemistry, Princeton University, Princeton, New Jersey 08544, USA. *These authors contributed equally to this work. Correspondence and requests for materials should be addressed to K.S.B. (email: kburch@physics.utoronto.ca).

Superconductivity can be produced locally in various materials by placing them in direct contact with a superconductor[1], resulting in unique combinations of distinct properties that do not coexist otherwise[2]. This proximity effect has been proposed as a powerful resource for practical applications in optoelectronics[3] and has been predicted to produce the elusive Majorana fermion[4] by combining a superconductor with a topological insulator (TI)[5–10]. These goals have been pursued actively, including the recent demonstrations of novel semiconductor light sources[11] and induced superconductivity in TIs[12–16] such as Bi_2Se_3 and Bi_2Te_3, which have been shown to have topologically protected surface states[17–19]. Nonetheless, all such experiments performed to date have employed low critical-temperature (low-T_c) materials that require extreme cooling, and the important ratio of the superconducting gap to the Fermi energy in such systems is very small. Inducing superconductivity with the larger energy scales and higher temperatures possible in high critical-temperature (high-T_c) superconductors[20] can enable future realizations of more practical devices, as well as greatly expand the ability to study the underlying physical phenomena[21].

A widely used approach for the demonstration of proximity-induced superconductivity in larger-scale devices is based on conductance spectra at superconducting–normal (S–N) interfaces[22]. The proximity-induced superconductivity was established in low-T_c junctions with a metal[23,24], or a semiconductor[25,26] as the N-contact. Specifically, Andreev reflection features with the width corresponding to the induced gap in the normal material, along with a reduced gap in the superconductor, were shown to manifest the signature of the proximity effect[23,24,27,28]. Low-T_c superconductivity has been observed recently in $Cu_xBi_2Se_3$[29–31], and a corresponding theory of unconventional superconductivity has been developed[32,33]. These low-T_c studies provide the evidence for existence of interactions in TIs, enabling the possibility of inducing a superconducting gap in TIs in proximity with high-T_c materials as well.

Here we generate proximity-induced superconductivity in Bi_2Se_3 and Bi_2Te_3 by combining them with a high-T_c superconductor, $Bi_2Sr_2CaCu_2O_{8+\delta}$ (Bi-2212), and characterize the induced superconductivity by studying the resulting current and differential conductance across the interface. Andreev reflection is observed as an excess current and an increase in differential conductance when cooling below T_c. The widths of the central features in the Andreev spectra do not reflect the full gap of Bi-2212, but rather the induced gap in the Bi_2Se_3 and Bi_2Te_3 due to the proximity effect. Furthermore, we observe additional features in the Andreev spectrum due to the reduced gap in the Bi-2212 at the interface—consistent with previous studies of the proximity effect with low-T_c superconductors[23,24,27,28]. This is a natural consequence of the extension of the superconducting order parameter into the Bi_2Se_3 and Bi_2Te_3, and confirms the existence of the proximity effect in our junctions. The Andreev scattering spectrum we observe shows good agreement with a recently developed d-wave theory[34], modified to account for the high-T_c order parameter profile in the proximity region.

Results

Sample characteristics. High-quality bulk Bi_2Se_3, Bi_2Te_3 and optimally doped Bi-2212 crystals were cleaved, resulting in atomically flat surfaces over large areas (Fig. 1a and b), and were subsequently mechanically bonded (Fig. 1c-f) in a dry atmosphere. These low-resistance tunnel junctions were then probed by conductance spectroscopy measurements, including the current and differential conductance versus voltage (Fig. 1g). The conductance spectroscopy experiments were performed using four-point probe measurements in a liquid He flow cryostat at different temperatures ranging from 295 to 4.5 K. Our mechanically bonded tunnel junction method was also verified to perform successfully on a Bi-2212/graphite junction (Supplementary Fig. S1), resulting in a typical S–N tunnelling spectra seen previously for Bi-2212, with point contact or scanning tunnelling microscopy[35].

Bi-2212/Bi_2Se_3 experiments. The first set of experiments was performed on Bi-2212/Bi_2Se_3 junctions. DC current along the c axis versus voltage (I–V) characteristics (Fig. 2a) reveal excess current below the Bi-2212 T_c (~85 K) due to the Andreev reflection at the S–N interfaces[36], consistent with the model developed for anisotropic superconductors[34]. The observed Andreev reflection indicates that we have achieved a surprisingly low barrier between Bi-2212 and Bi_2Se_3. Furthermore, this is the key mechanism for the superconducting proximity effect[37], suggesting the existence of a proximity-induced superconducting region at the Bi-2212/Bi_2Se_3 interface. Just below T_c, the excess current, I_e, reaches the maximal value similar to the normal–normal (N–N) interface current (measured for $T > T_c$), resulting in total current nearly twice that of the N–N interface due to the contribution of the Cooper pairs when Andreev reflection occurs. A different measurement—AC differential conductance below T_c, $(dI/dV)_S$, divided by the normal state conductance$(dI/dV)_N$ measured at 105 K, confirms the DC I–V measurement. Specifically, the AC differential conductance reveals a zero-bias conductance peak due to Andreev reflection below T_c (Fig. 2b). At lower temperatures (around 60 K), reduction of higher-bias current was observed, and at the same temperatures, additional higher-bias features appeared in the differential conductance measurement. These features result from the gap reduction in Bi-2212 and the induced gap in Bi_2Se_3. However, the detailed structure of these spectral features could be studied only at lower temperatures as discussed in detail below.

To demonstrate the spectral features more clearly, we performed both DC and AC measurements at temperatures well below T_c. DC I–V characteristics of the junction (Fig. 2c) show excess current at lower voltages up to about 13 mV with a correspondingly smaller value I_S ~2.7 μA. However, two additional step-like features appear near 27 and 45 mV. These features are confirmed by an AC differential conductance measurement (Fig. 2d), showing a wide conductance feature between −13 and +13 mV, as well as peaks at ±27 and ±45 mV, in good quantitative agreement with the DC measurement (Fig. 2c inset). Similar results were obtained with Bi-2212/Bi_2Te_3 junctions as described below. This conductance spectrum is a clear signature of a proximity-induced superconducting region in the Bi_2Se_3.

When the proximity effect occurs (Fig. 3a), a superconducting gap is induced in the normal material, Δ_i, and near the interface, the gap in the superconducting material is reduced from the intrinsic value, Δ_0 (Fig. 3b), to a smaller one, Δ_r[1,23,24,27,28]. Generally, the superconducting gap is position-dependent along the axis normal to the interface plane, $\Delta(x)$, and Andreev-scattering probability is finite in the whole proximity region. However, the scattering can be divided into two main energy ranges: electrons (holes) with energy $|E| < \Delta_i$ will be mainly Andreev-reflected inside the proximity-induced superconducting region of the normal material, whereas electrons (holes) with $\Delta_i < |E| < \Delta_r$ will continue to the S–N interface and then Andreev-reflect, mainly near the material interface. Thus, conductance spectrum taken on an interface exhibiting the proximity effect will show Andreev-scattering features corresponding to both gaps[23,24,27,28]. In our experiments, therefore, the central conductance peak is a manifestation of Andreev reflection from the normal region to the proximity-induced superconducting region of Bi_2Se_3 with a gap Δ_i~13 mV. The reduced gap in Bi-2212 due to the proximity effect appears as a conductance peak at Δ_r~27 mV. The change in the zero-bias conductance with temperature is an additional manifestation of the Andreev scattering. Indeed, just below T_c, the zero-bias conductance increases to nearly twice its value above T_c (Fig. 3c). This temperature dependence, as well

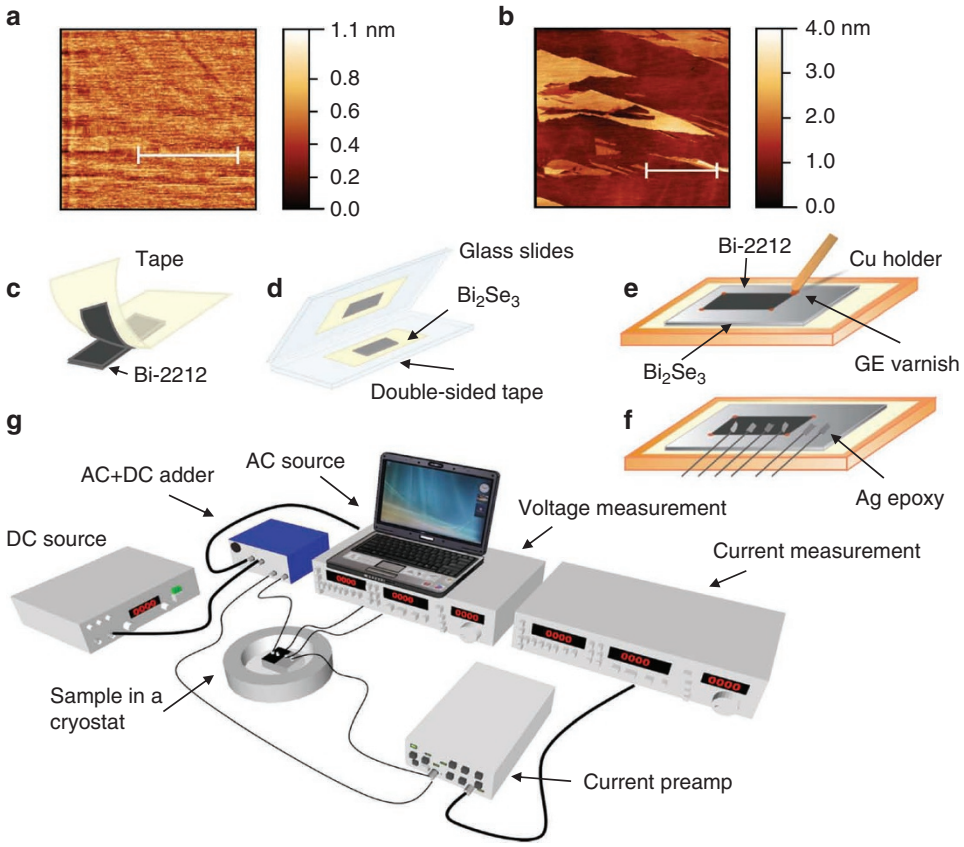

Figure 1 | Device fabrication and measurement set-up. (**a**) Atomic force microscope (AFM) image of the crystal surface of Bi_2Se_3. The scale bar corresponds to 2 μm. (**b**) Larger area AFM scan of the Bi_2Te_3 sample, demonstrating the vertical inhomogeneity of the surface is limited to ±2 unit cells. The scale bar corresponds to 3 μm. Junction fabrication technique: (**c**) Bi-2212 (BSCCO) crystal is cleaved using scotch tape. (**d**) Bi_2Se_3 (or Bi_2Te_3) is sandwiched between glass slides with double-sided tapes and the top glass slide is lifted off, cleaving a flat surface. (**e**) The Bi_2Se_3 (or Bi_2Te_3) is transferred to a Cu sample holder, and the cleaved Bi-2212 crystal is applied to Bi_2Se_3 or Bi_2Te_3 using GE varnish at the corners. (**f**) Contacts are made with Ag epoxy or evaporated Au/Ti. (**g**) Experimental set-up: four-point DC current-voltage and AC differential conductance measurements performed down to 4.5 K, using a liquid He-flow cryostat with lock-in amplifiers. DC bias from the power supply is combined with the AC signal from the voltage lock-in amplifier in a transformer-based adder.

as the spectral shape of the conductance at various temperatures (Fig. 3c inset), completely rules out any possible heating-related effects, whereas a junction with an increased barrier exhibits no proximity (Fig. 3d). Andreev reflection between Bi-2212 and normal Bi_2Se_3 (or Bi_2Te_3) with no proximity would have appeared as a single Andreev feature with a width corresponding to the full gap of Bi-2212, which is completely different from our observations. The full gap appears in our experiment as additional peaks at Δ_0~45 mV, whose magnitude and temperature dependence are quantitatively consistent with previous tunnelling studies of Bi-2212 (ref. 35) and our high-barrier junctions (Fig. 3d).

The zero-bias conductance feature has a number of characteristics consistent with Andreev reflection in a proximity-induced region. The height of the Bi_2Se_3 Andreev zero-bias conductance feature is nearly twice the normal conductance value due to the Cooper pair contribution (Figs 2d and 3c), whereas the width is determined by the induced superconducting gap, $2\Delta_i$. The width of the Andreev feature is also manifested in the excess current up to a negative bias Δ_i in the DC I–V characteristic (Fig. 2c)—nearly twice as high as the current in the normal state (Fig. 2a). The probability of Andreev scattering at the interface with the Bi-2212 is reduced by the scattering in Bi_2Se_3, resulting in slightly smaller contribution to the conductance at Δ_r. At low temperatures, both the induced gap and the reduced gap features in differential conductance result in a step-like I–V curve (Fig. 2c). With increasing temperature, the features in the differential conductance merge into one wide central peak (Fig. 2b) and the step-like structure in I–V disappears (Fig. 2a). Therefore, at certain higher temperatures, the total excess current can be larger than at lower temperatures.

Theoretical modelling. For the quantitative theoretical modelling of the effect, we calculated the c axis Bi-2212/Bi_2Se_3 and Bi-2212/Bi_2Te_3 conductance spectra using the S–N transport formalism developed for anisotropic superconductors[34]. The differential conductance below T_c $(dI/dV)_S$, divided by the normal state conductance $(dI/dV)_N$ is given by the half-sphere integration over solid angle[38] Ω:

$$\sigma(E) = \frac{\int d\Omega \sigma_N \cos\theta_N \sigma_R(E)}{\int d\Omega \sigma_N \cos\theta_N}, \quad (1)$$

where E is the quasiparticle energy and θ_N is the incidence angle (relative to the interface normal) in the normal material, σ_N is the conductance from normal to normal material with the same geometry, and

$$\sigma_R(E) = \frac{1+\sigma_N|\kappa_+|^2+(\sigma_N-1)|\kappa_-\kappa_+|^2}{|1+(\sigma_N-1)|\kappa_-\kappa_+|\exp(i\varphi_- - i\varphi_+)|^2}, \quad (2)$$

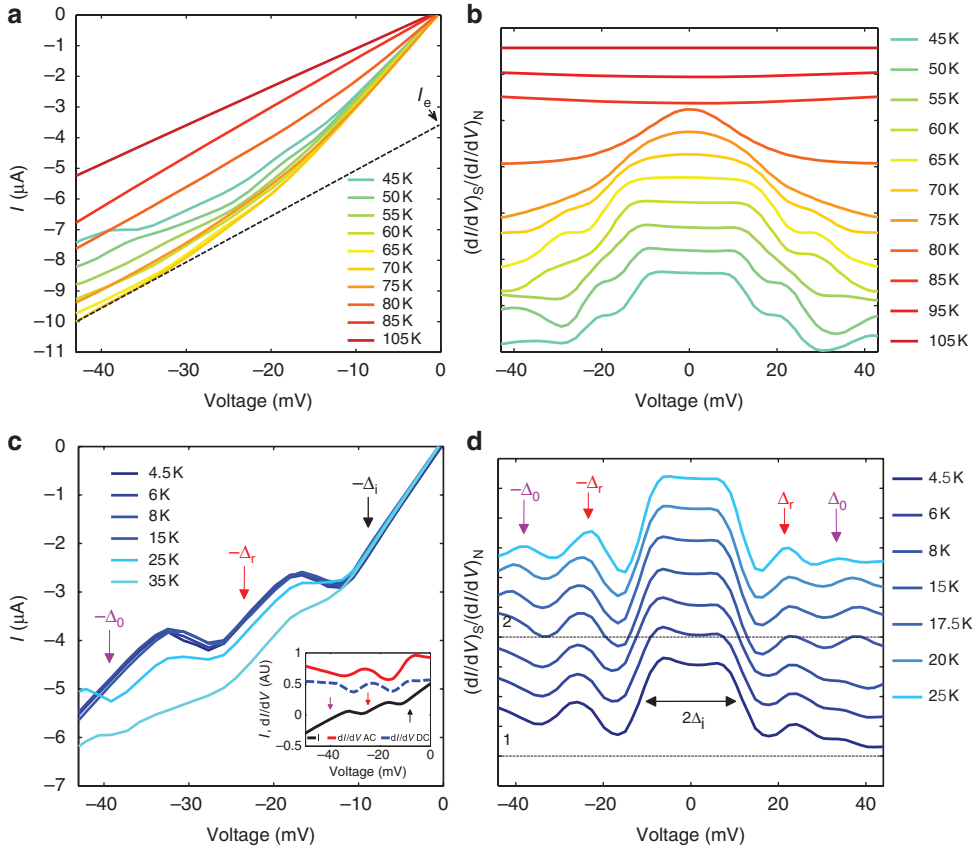

Figure 2 | Bi-2212/Bi_2Se_3 junction measurements. (**a**) DC current–voltage characteristics of the low-resistance Bi-2212/Bi_2Se_3 junction for different temperatures above and below T_c. Below T_c, excess current typical of Andreev reflection at an S–N interface is exhibited. The 70 K I–V curve shows the maximal excess current I_e ~4.85 μA—similar to the value of the normal junction (above T_c) at the voltage where the superconducting state current becomes linear (black dashed line). The total excess current is smaller for lower temperatures due to additional gap features. (**b**) AC differential conductance$(dI/dV)_S$, normalized by the normal state conductance $(dI/dV)_N$ at 105 K, for the low-resistance Bi-2212/Bi_2Se_3 junction at different temperatures above and below T_c. A zero-bias conductance Andreev peak is clearly seen below T_c, with additional features in the spectrum appearing at lower temperatures. The curves are shifted for clarity. (**c**) DC current–voltage characteristics of the low-resistance Bi-2212/Bi_2Se_3 junction for different temperatures well below T_c. In addition to the excess current, the low-temperature curves exhibit two distinct steps corresponding to the dips in the differential conductance measured for AC bias. The black arrow shows the induced Bi_2Se_3 gap, Δ_i, with a current twice that of the normal state at the same voltage (**a**), and the red arrow indicates the reduced Bi-2212 gap, Δ_r, whereas the intrinsic Bi-2212 gap, Δ_0, is shown by purple arrows. The inset shows the DC and the AC differential conductance at 4.5 K, indicating the good correspondence between the different measurements of Δ_0 (purple arrow), Δ_r (red arrow) and Δ_i (black arrow); AU, arbitrary units. (**d**) AC differential conductance $(dI/dV)_S$, normalized by the normal state conductance $(dI/dV)_N$ at 105 K, for a low-resistance Bi-2212/Bi_2Se_3 junction for different temperatures well below T_c. The curves are shifted for clarity. The zero-bias conductance feature is due to the Andreev reflection between the normal and proximity-induced superconducting regions in Bi_2Se_3, where the width of the peak is nearly $2\Delta_i$. The two additional peaks indicate the reduced and the intrinsic Bi-2212 gaps.

where $\kappa_\pm = \left[E - \sqrt{E^2 - |\Delta_\pm|^2}\right] / |\Delta_\pm|$ and $\Delta_\pm = |\Delta_\pm| \exp(i\varphi_\pm)$—electron-like and hole-like quasiparticle effective pair potentials with the corresponding phases $i\varphi_\pm$.

In case of c axis tunnelling, the hole-like and the electron-like quasiparticles transmitted into the superconductor experience the same effective pair potentials, which have similar dependence on the azimuthal angle α in the *ab* plane $\Delta_+ = \Delta_- = \Delta_0 \cos(2\alpha)$. The total Andreev reflection spectrum is obtained by calculating the reflection and the transmission in the proximity region, followed by reflection at the interface between the two materials. The calculated spectra in this two-stage scattering model with the modified gaps as fit parameters show good agreement with the experimental conductance measurements (Fig. 3e).

Bi-2212/Bi_2Te_3 experiments. To demonstrate the wide applicability of our mechanical bonding technique, we have constructed similar S–N junctions combining Bi-2212 from a different batch of crystals and Bi_2Te_3 grown by a different group (Princeton University) than that producing the Bi_2Se_3 (Rutgers University). Conductance measurements of low-barrier Bi-2212/Bi_2Te_3 junctions also clearly show the proximity-induced gap in Bi_2Te_3, as well as the reduced gap in Bi-2212 (Fig. 4a). The central Andreev feature due to the induced gap in the spectrum also appears immediately below T_c similar to Bi_2Se_3, with a conductance increase of nearly twice the normal value (Fig. 4b), and a width consistent with Andreev reflection in the proximity-induced region. We have constructed several Bi-2212/Bi_2Te_3 junctions with various induced gap sizes, and the measured spectra agree well with the calculations (Fig. 4b inset). One of the Bi-2212/Bi_2Te_3 junctions exhibited particularly large proximity-induced features in differential conductance (Fig. 4c), and the corresponding current-voltage DC measurement shows excess current as high as 90 μA (Fig. 4d). The proximity-related Andreev features and the excess current were observed repeatedly in several Bi-2212/Bi_2Se_3 (Fig. 4e) and Bi-2212/Bi_2Te_3 (Fig. 4f) devices.

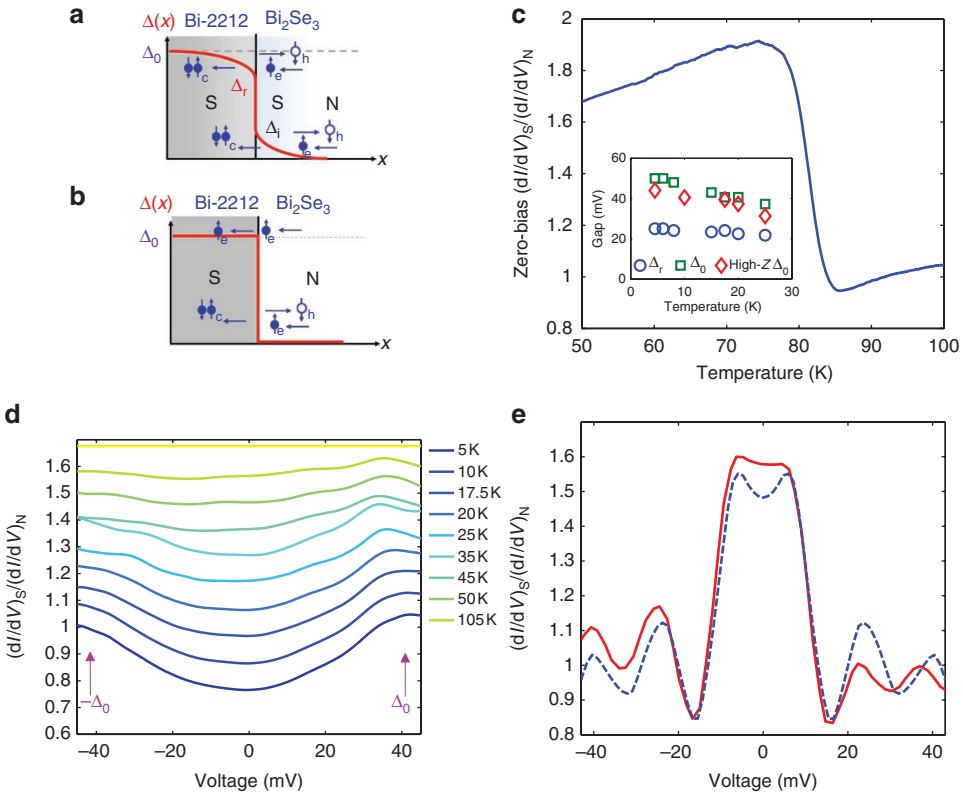

Figure 3 | Proximity induced superconductivity. A schematic drawing of the junction in two regimes: (**a**) low-resistance with proximity induced superconductivity in Bi_2Se_3 (or Bi_2Te_3). Andreev scattering takes place in the whole proximity region with lower energy particles reflected mainly in Bi_2Se_3 (or Bi_2Te_3), and higher energy ones mainly at the interface with Bi-2212; (**b**) high-resistance with no proximity-induced superconductivity in Bi_2Se_3 (or Bi_2Te_3)—quasiparticle scattering occurs at the interface. (**c**) Temperature dependence of the zero-bias differential conductance for Bi-2212/Bi_2Se_3. Below T_c, the Andreev process enhances the conductance by almost a factor of 2. The inset shows the temperature dependence of the reduced Bi-2212 gap Δ_r blue circles), and the intrinsic Bi-2212 gap Δ_0 in the low-resistance junction (green squares) and in the high-resistance junction (red diamonds). (**d**) Differential conductance $(dI/dV)_S$, normalized by the normal state conductance $(dI/dV)_N$ at 105 K, for a high-resistance Bi-2212/Bi_2Se_3 junction for different temperatures, demonstrating the typical quasiparticle tunnelling differential conductance, resulting in a conductance dip in the gapped region. The curves are shifted for clarity. The arrows indicate the intrinsic superconducting gap of Bi-2212, $\pm\Delta_0$, around 45 mV. (**e**) Measured (solid red line) and calculated (dashed blue line) 15 K differential conductance $(dI/dV)_S$, normalized by the normal state conductance $(dI/dV)_N$ at 105 K, for a low-resistance Bi-2212/Bi_2Se_3.

Discussion

To rule out alternative interpretations of our results, we considered various complications caused by the planar geometries of our devices, which are different from those based on point contacts that guarantee ballistic transport. In planar junctions, electron scattering can slightly affect the ballistic nature of the transport. This could have some effect on our measurements; nonetheless, it can only result in the observation of features at voltages that are a little higher than the true electron energies. However, this cannot produce an Andreev feature that is narrower than the true gap of the system. Furthermore, this effect cannot produce additional features in the spectra that we observe, which are consistent with the reduced gap at the interface. Moreover, to the extent that this effect is relevant, it could result in a measured bulk Bi-2212 gap that is bigger than the known gap size from photoemission and tunnelling studies. However, we observe a bulk gap in accord with previous measurements and that is fairly insensitive to the details of the contact (see Supplementary Discussion and Supplementary Fig. S2).

Previous low-T_c S–N planar-junction conductance experiments[25] showed a narrow and small zero-bias conductance peak (several percent increase) due to pair currents. Later, a more detailed interpretation was suggested with a more complex Andreev reflection process including an electron-hole phase conjugation[39]. This phase conjugation model, however, predicts a rapid monotonic decrease of conductance at non-zero bias due to the different phases accumulated by quasiparticles. Therefore, this model is not applicable to the wide spectral features with complex shapes corresponding to the Andreev reflection at the induced gap interface observed in our experiments and in previous low-T_c work[23,24,27,28]. Moreover, our experimental results are also different from the low-T_c results[25,39]. Our measurements show a proximity-induced gap feature with a wide region, appearing immediately below T_c with almost twice the normal conductance (Figs 3c and 4b). Furthermore, our measured Andreev spectra show several distinct features related to the induced gap in the normal material and the reduced gap in the superconductor (similar to ref. 28). At lower temperatures, the central feature in our measured spectra is almost independent of the bias, which is consistent with the proximity-induced gap and different from the phase-conjugation model[39].

Moreover, any possible *ab*-plane tunnelling in our devices can be ruled out for a number of experimental reasons. First, the areal coverage is much greater for c axis tunnelling then for *ab*-plane tunnelling. In fact, when the TI surfaces were rougher, we found no proximity effects, confirming that additional area for any possible *ab*-plane tunnelling did not change the spectra significantly. Second, in bulk Bi-2122, the c axis resistivity is very high only in the normal state, whereas in the superconducting state, all directions reveal zero resistance. Therefore, as the area perpendicular to the

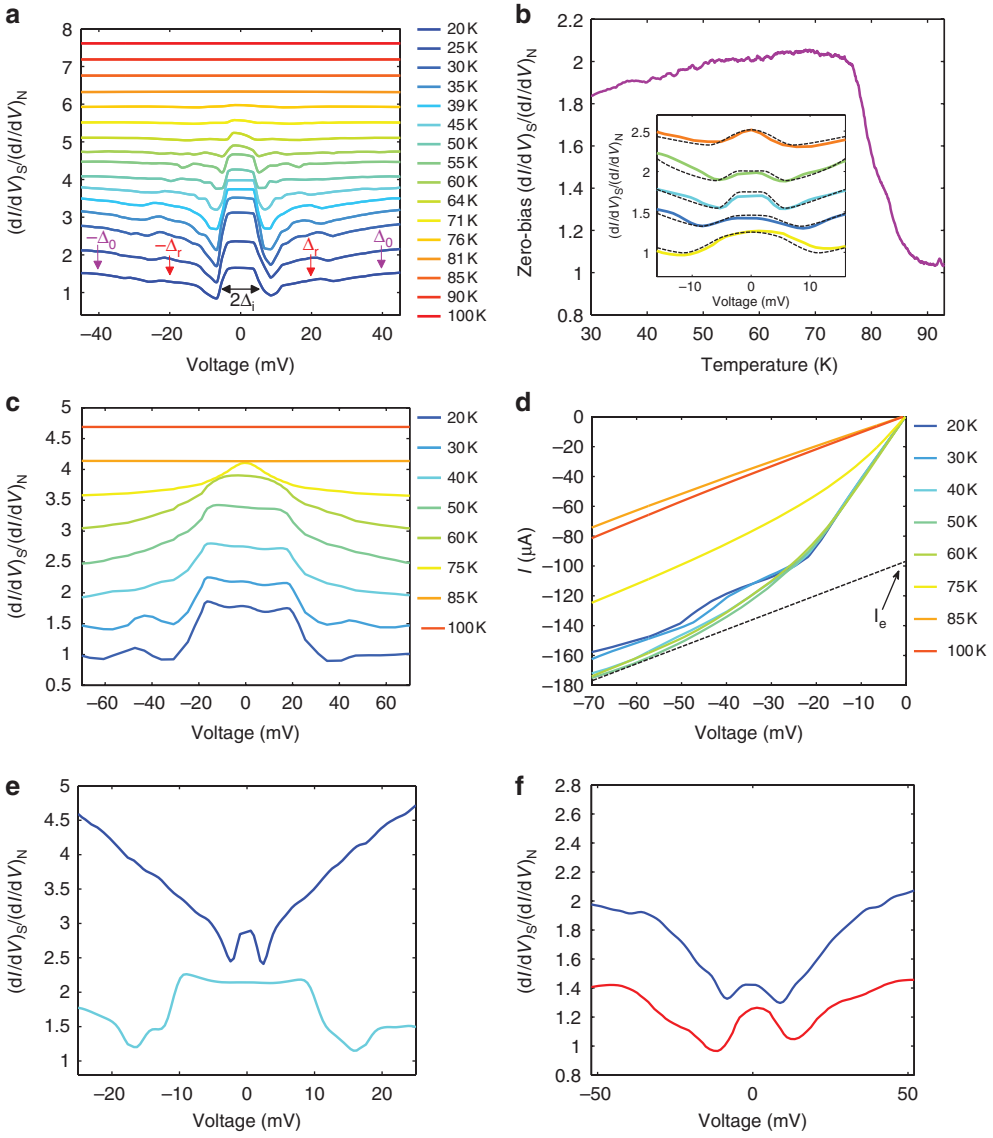

Figure 4 | Bi-2212/Bi_2Te_3 junction measurements. (**a**) AC differential conductance$(dI/dV)_S$, normalized by the normal state conductance $(dI/dV)_N$ at 100 K, for a low-resistance Bi-2212/Bi_2Te_3 junction at different temperatures above and below T_c. The curves are shifted for clarity. (**b**) Temperature dependence of the zero-bias differential conductance for Bi-2212/Bi_2Te_3. Below T_c, the Andreev process enhances the conductance by almost a factor of 2. The inset shows 10 K measured (solid lines) and calculated (dashed lines) normalized differential conductance for several Bi-2212/Bi_2Te_3 devices with different values of the induced gap size. (**c**) AC differential conductance$(dI/dV)_S$, normalized by the normal state conductance $(dI/dV)_N$ at 100 K, for a large-induced-gap Bi-2212/Bi_2Te_3 junction at different temperatures. The curves are shifted for clarity. (**d**) DC current–voltage characteristics of the large-induced-gap Bi-2212/Bi_2Te_3 junction, for different temperatures above and below T_c. (**e**) Measured normalized differential conductance for two Bi-2212/Bi_2Se_3 devices with different values of the induced gap size. The curves are shifted for clarity (**f**) Measured normalized differential conductance for two Bi-2212/Bi_2Te_3 devices with different values of the induced gap size. The curves are shifted for clarity.

c axis is much larger than the exposed area normal to the *ab* plane, the overall current is along the c axis, eliminating any possible *ab*-plane effects. Last, our c axis tunnelling conductance measurements are very different from an *ab*-plane Andreev-bound state peak[40]. Specifically, our differential conductance measurements reveal a very wide central Andreev feature, which is almost independent of the bias. This is consistent with Andreev reflection in the normal material from an induced gap and is completely different from an Andreev-bound state. Furthermore, an Andreev-bound state-related peak in conductance should have a height that is independent of the barrier strength—*Z*. However, in our case, increasing *Z* results in a very different conductance spectrum shape. This is consistent with elimination of a proximity region at high *Z* and is inconsistent with a bound state.

To further verify that the Andreev scattering is due to the proximity-induced superconductivity in Bi_2Se_3, and dismiss any possible processes occurring in Bi-2212 alone, the Bi-2212/Bi_2Se_3 junction barrier was increased mechanically. Rapidly heating the junction to 300 K and cooling it back to 4 K in less than 30 min made it possible to achieve this. As expected, the differential conductance measurement performed on the high-resistance junction revealed only spectra typical of a c axis tunnelling measurement on Bi-2212 (ref. 35), indicating the lack of a proximity effect. Specifically, the superconducting gap of Bi-2212 was observed; however, no Andreev peak appeared at the Bi-2212 reduced gap Δ_r, and no conductance features corresponding to the proximity-induced gap in the Bi_2Se_3 were observed (Fig. 3d). The differential conductance spectrum for the high-resistance junction showed the superconducting gap of

Bi-2212, Δ_0, and its temperature dependence agrees with the values from the low-resistance junction measurement (Fig. 3c inset) as well as for the graphite junction (Supplementary Fig. S1), confirming the origin of the conductance peaks.

Our results present clear evidence of proximity-induced high-T_c superconductivity in Bi_2Se_3 and Bi_2Te_3. We achieved this via our newly developed technique of mechanically bonded junctions and confirmed it by various experiments. Specifically below T_c, we observed Andreev features corresponding to a reduced gap of Bi-2212 appearing concurrently with an induced gap in Bi_2Se_3 or Bi_2Te_3. The disappearance of these features in the same junctions when the barrier is increased further confirms that the proximity effect is the origin of these features. The proximity-induced superconductivity in Bi_2Se_3 and Bi_2Te_3 is demonstrated at temperatures at least an order of magnitude higher than previously reported results. The developed mechanical bonding technique may render various future experiments on novel materials, including high-T_c superconductors and TIs feasible. Furthermore, our proximity demonstration paves the way for practical realization of TI-based devices involving superconductivity, including Majorana fermion-based topological quantum computing.

Methods

Device fabrication. High-quality bulk Bi_2Se_3 and Bi_2Te_3 crystals were prepared as described elsewhere[41]. In addition, optimally doped $Bi_2Sr_2CaCu_2O_{8+\delta}$ (Bi-2212) crystals ($T_c \approx 85$ K) were grown by the floating-zone method[42]. Bi-2212/Bi_2Se_3 and Bi-2212/Bi_2Te_3 junctions were fabricated by using these crystals as the starting materials. The formation of atomically smooth surfaces via cleaving is well established for Bi-2212, Bi_2Te_3 and Bi_2Se_3. Bi-2212 was cleaved in a dry nitrogen-purged box with adhesive tape (Fig. 1c), producing a clean, flat piece of Bi-2212 a few hundred micrometres thick. However, we have found the Bi_2Te_3 and Bi_2Se_3 surfaces were not smooth enough when simply cleaved using scotch tape. Thus, we cleaved a bulk Bi_2Se_3 or Bi_2Te_3 crystal in the dry box by sandwiching the crystal between two glass slides with double-sided tape. After applying slight pressure to the glass slides, the top glass slide was lifted off (Fig. 1d). This approach was taken due to the difficulty of producing flat surfaces by cleaving Bi_2Se_3 or Bi_2Te_3 with scotch tape, as was done for Bi-2212. Next, the Bi_2Se_3 or Bi_2Te_3 was transferred to a Cu sample holder by attaching a double-sided tape to the Cu and placing one of the glass slides with Bi_2Se_3 or Bi_2Te_3 on the sample holder. By lifting off the glass slide, a smooth and fresh surface of Bi_2Se_3 or Bi_2Te_3 was left on the sample holder. The Bi-2212 was then attached to the Bi_2Se_3 or Bi_2Te_3 by placing the Bi-2212 on the Bi_2Se_3 or Bi_2Te_3, applying GE varnish on the corners of Bi-2212 (Fig. 1e). In the fabrication process, no pressure is required and the junction is formed spontaneously. The important point is cleaving the materials in a dry and inert atmosphere (a nitrogen-purged glove box in our case) with a technique that ensures large, atomically smooth surfaces. Contacts were made on the sample using Cu wires and Ag epoxy or Ti/Au (Fig. 1f). This method was inspired by the mechanical exfoliation technique; however, no exfoliation is needed here, and bulk-cleaved crystals are attached mechanically using GE varnish on the corners. Low-barrier junctions were only revealed when the Bi_2Se_3 and Bi_2Te_3 were cleaved using our glass-slide technique. When simply cleaving the samples with scotch tape, all junctions revealed high-barrier behaviour, specifically the resistance across the junction was high (greater than tens of kiloOhms at room temperature) and no Andreev features were observed upon cooling.

Measurement set-up description. In our set-up, four-point probe measurements were performed in a liquid He-flow cryostat at different temperatures ranging from 295 to 4.5 K. Bias-dependent differential conductance as well as current versus voltage were measured on the junctions using two lock-in amplifiers (Stanford Research Systems SR810), a DC voltage source (BK Precision 1787B), two DC multi-meters (Hewlett Packard 3457A and Agilent 34401A) and a home-built, shielded AC + DC adder box (Fig. 1g). One of the lock-in amplifiers was used to produce a small AC voltage output at a frequency near 1 kHz. The AC voltage was added to the DC output of a DC power supply using a transformer-based adder. A voltage was applied to the sample, with the resulting voltage measured with a lock-in (the AC part) and a multimetre (the DC part). At the same time, the current was converted to voltage, amplified with a pre-amplifier (SRS 570) and measured with another lock-in (AC) and a multimetre (DC).

References

1. de Gennes, P. G. *Superconductivity of Metals and Alloys*, Chapter 7 (Benjamin, New York, 1966).
2. Heersche, H. B., Jarillo-Herrero, P., Oostinga, J. B., Vandersypen, L. M. K. & Morpurgo, A. F. Bipolar supercurrent in graphene. *Nature* **446,** 56–59 (2007).
3. Asano, Y., Suemune, I., Takayanagi, H. & Hanamura, E. Luminescence of a Cooper Pair. *Phys. Rev. Lett.* **103,** 187001 (2009).
4. Fu, L. & Kane, C. L. Superconducting proximity effect and Majorana Fermions at the surface of a topological insulator. *Phys. Rev. Lett.* **100,** 096407 (2008).
5. Fu, L., Kane, C. L. & Mele, E. J. Topological insulators in three dimensions. *Phys. Rev. Lett.* **98,** 106803 (2007).
6. Bernevig, B. A., Hughes, T. L. & Zhang, S.- C. Quantum spin hall effect and topological phase transition in HgTe quantum wells. *Science* **314,** 1757–1761 (2006).
7. Moore, J. E. & Balents, L. Topological invariants of time-reversal-invariant band structures. *Phys. Rev. B* **75,** 121306(R) (2007).
8. Akhmerov, A. R., Nilsson, J. & Beenakker, C. W. J. Electrically detected interferometry of Majorana Fermions in a topological insulator. *Phys. Rev. Lett.* **102,** 216404 (2009).
9. Tanaka, Y., Yokoyama, T. & Nagaosa, N. Manipulation of the Majorana fermion, Andreev reflection, and Josephson current on topological insulators. *Phys. Rev. Lett.* **103,** 107002 (2009).
10. Linder, J., Tanaka, Y., Yokoyama, T., Sudbø, A. & Nagaosa, N. Unconventional superconductivity on a topological insulator. *Phys. Rev. Lett.* **104,** 067001 (2010).
11. Sasakura, H. *et al.* Enhanced photon generation in a Nb/n-InGaAs/p-InP superconductor/semiconductor-diode light emitting device. *Phys. Rev. Lett.* **107,** 157403 (2011).
12. Zhang, D. *et al.* Superconducting proximity effect and possible evidence for Pearl vortices in a candidate topological insulator. *Phys. Rev. B* **84,** 165120 (2011).
13. Sacepe, B. *et al.* Gate-tuned normal and superconducting transport at the surface of a topological insulator. *Nat. Commun.* **2,** 575 (2011).
14. Veldhorst, M. *et al.* Josephson supercurrent through a topological insulator surface state. *Nat. Mater.* **11,** 417–421 (2012).
15. Yang, F. *et al.* Proximity effect at superconducting Sn-Bi_2Se_3 interface. *Phys. Rev. B* **85,** 104508 (2012).
16. Wang, M.- X. *et al.* The coexistence of superconductivity and topological order in the Bi_2Se_3 thin films. *Science* **336,** 52–55 (2012).
17. Xia, Y. *et al.* Observation of a large-gap topological-insulator class with a single Dirac cone on the surface. *Nature Phys.* **5,** 398–402 (2009).
18. Chen, Y. L. *et al.* Experimental realization of a three-dimensional topological insulator, Bi_2Te_3. *Science* **325,** 178–181 (2009).
19. Zhang, H. *et al.* Topological insulators in Bi_2Se_3, Bi_2Te_3 and Sb_2Te_3 with a single Dirac cone on the surface. *Nature Phys.* **5,** 438–442 (2009).
20. Lee, P. A., Nagaosa, N. & Wen, X.- G. Doping a Mott insulator: physics of high temperature superconductivity. *Rev. Mod. Phys.* **78,** 17–85 (2006).
21. Bozovic, I. *et al.* Giant proximity effect in cuprate superconductors. *Phys. Rev. Lett.* **93,** 157002 (2004).
22. Guéron, S., Pothier, H., Birge, N. O., Esteve, D. & Devoret, M. H. Superconducting proximity effect probed on a mesoscopic length scale. *Phys. Rev. Lett.* **77,** 3025–3028 (1996).
23. van Son, P. C., van Kempen, H. & Wyder, P. New method to study the proximity effect at the normal-metal–superconductor interface. *Phys. Rev. Lett.* **59,** 2226–2228 (1987).
24. Wolf, E. L. Proximity effect tunneling. *Physica B+C* **109, 110B,** 1722–1736 (1982).
25. Kastalsky, A. *et al.* Observation of pair currents in superconductor-semiconductor contacts. *Phys. Rev. Lett.* **67,** 3026–3029 (1991).
26. Nguyen, C., Kroemer, H. & Hu, E. L. Anomalous Andreev conductance in InAs-AlSb quantum well structures with Nb electrodes. *Phys. Rev. Lett.* **69,** 2847–2850 (1992).
27. Nishino, T., Hatano, M., Hasegawa, H., Kure, T. & Murai, F. Carrier reflection at the superconductor-semiconductor boundary observed using a coplanar-point-contact injector. *Phys. Rev. B* **41,** 7274–7276 (1990).
28. Heslinga, D. R., Shafranjuk, S. E., van Kempen, H. & Klapwijk, T. M. Observation of double-gap-edge Andreev reflection at Si/Nb interfaces by point-contact spectroscopy. *Phys. Rev. B* **49,** 10484–10494 (1994).
29. Wray, L. A. *et al.* Observation of topological order in a superconducting doped topological insulator. *Nat. Phys.* **6,** 855–859 (2010).
30. Kriener, M., Segawa, K., Ren, Z., Sasaki, S. & Ando, Y. Bulk superconducting phase with a full energy gap in the doped topological insulator $Cu_xBi_2Se_3$. *Phys. Rev. Lett.* **106,** 127004 (2011).
31. Sasaki, S. *et al.* Topological superconductivity in $Cu_xBi_2Se_3$. *Phys. Rev. Lett.* **107,** 217001 (2011).
32. Hsieh, T. H. & Fu, L. Majorana fermions and exotic surface Andreev bound states in topological superconductors: application to $Cu_xBi_2Se_3$. *Phys. Rev. Lett.* **108,** 107005 (2012).
33. Yamakage, A., Yada, K., Sato, M. & Tanaka, Y. Theory of tunneling conductance and surface-state transition in superconducting topological insulators. *Phys. Rev. B* **85,** 180509(R) (2012).
34. Kashiwaya, S., Tanaka, Y., Koyanagi, M. & Kajimura, K. Theory for tunneling spectroscopy of anisotropic superconductors. *Phys. Rev. B* **53,** 2667–2676 (1996).

35. Renner, C. & Fischer, O. Vacuum tunneling spectroscopy and asymmetric density of states of $Bi_2Sr_2CaCu_2O_{8+\delta}$. *Phys. Rev. B* **51,** 9208–9218 (1995).
36. Blonder, G. E., Tinkham, M. & Klapwijk, T. M. Transition from metallic to tunneling regimes in superconducting microconstrictions: excess current, charge imbalance, and supercurrent conversion. *Phys. Rev. B* **25,** 4515–4532 (1982).
37. Pannetier, B. & Courtois, H. Andreev reflection and proximity effect. *J. Low Temp. Phys.* **118,** 599–615 (2000).
38. Yamashiro, M., Tanaka, Y., Tanuma, Y. & Kashiwaya, S. Theory of tunneling conductance for normal metal/insulator/triplet superconductor junction. *J. Phys. Soc. Japan* **67,** 3224–3233 (1998).
39. van Wees, B. J., de Vries, P., Magnée, P. & Klapwijk, T. M. Excess conductance of superconductor-semiconductor interfaces due to phase conjugation between electrons and holes. *Phys. Rev. Lett.* **69,** 510–513 (1992).
40. Tanaka, Y. & Kashiwaya, S. Theory of tunneling spectroscopy of d-wave superconductors. *Phys. Rev. Lett.* **74,** 3451–3454 (1995).
41. Analytis, J. G. *et al.* Bulk Fermi surface coexistence with Dirac surface state in Bi_2Se_3: a comparison of photoemission and Shubnikov–de Haas measurements. *Phys. Rev. B* **81,** 205407 (2010).
42. Gu, G. D., Takamuku, K., Koshizuka, N. & Tanaka, S. Growth and superconductivity of $Bi_{2.1}Sr_{1.9}Ca_{1.0}(Cu_{1-y}Fe_y)_2O_x$ single crystal. *J. Cryst. Growth* **137,** 472–478 (1994).

Acknowledgements

The work at the University of Toronto was supported by the Natural Sciences and Engineering Research Council of Canada, the Canadian Foundation for Innovation, and the Ontario Ministry for Innovation. The work at Rutgers was supported by National Science Foundation DMR-1104484. The crystal growth at Princeton was supported by the US National Science Foundation, grant number DMR-0819860.

Author contributions

P.Z. and A.H. equally contributed to this work. P.Z., A.H. and K.S.B. planned the research. S.Y.F.Z. and A.J. implemented the conductance measurement set-up. A.H. and M.K. carried out the theoretical modelling. D.C.K., N.L., S.-W.C., Z.X., A.Y., G.D.G., S.J., and R.J.C. grew the crystals for the devices. P.Z. and A.H. performed the experiments and wrote the paper. K.S.B. conceptualized the experiment and supervised the work.

Additional information

Supplementary Information accompanies this paper at http://www.nature.com/naturecommunications

Competing financial interests: The authors declare no competing financial interests.

Reprints and permission information is available online at http://npg.nature.com/reprintsandpermissions/

How to cite this article: Zareapour, P. *et al.* Proximity-induced high-temperature superconductivity in the topological insulators Bi_2Se_3 and Bi_2Te_3. *Nat. Commun.* 3:1056 doi: 10.1038/ncomms2042 (2012).